Innovative Food Science and Emerging Technologies 75 (2022) 102910

Contents lists available at ScienceDirect

Innovative Food Science and Emerging Technologies

journal homepage: www.elsevier.com/locate/ifset

Improving the texture and rheological qualities of a plant-based fishball analogue by using konjac glucomannan to enhance crosslinks with soy protein

Xinli Ran [a], Xiaowei Lou [b], Haiqi Zheng [b], Qingyin Gu [b], Hongshun Yang [a,b,*]

[a] Department of Food Science & Technology, National University of Singapore, Singapore 117542, Singapore
[b] National University of Singapore (Suzhou) Research Institute, 377 Lin Quan Street, Suzhou Industrial Park, Suzhou, Jiangsu 215123, PR China

ARTICLE INFO

Keywords:
Plant-based seafood analogue
Konjac glucomannan
Texture
Viscoelasticity
Microstructure
Protein-polysaccharide interaction

ABSTRACT

Global fisheries pressure generates interest in sustainable seafood production and developing plant-based seafood. This study took fishball as an example of seafood products applying konjac glucomannan (KGM) in developing plant-based fishball (PFB) analogues mimicking the texture of fishball. Increasing KGM concentration (up to 8.0%) influenced texture and rheological properties of PFB progressively, where the hardness, chewiness, and gel strength of PFB were significantly enhanced. Decreased pH value (9.38 to 7.93) and increased α-helix, β-sheet, and helix/coil ratio (1.40 to 1.70%) validated a promotion of hydrogen bonds and ordered structures by KGM. The strengthened interaction strength and hydrogen bonds formed at -OH groups of KGM and amide linkage of soy protein could be responsible for textural improvement. A more compact and regular microstructure also validated a firmer texture in PFB with higher KGM levels. Besides, KGM (3.5–8.0%) significantly decreased instantaneous compliance J_0 (101.3×10^{-6} to 58.1×10^{-6} Pa^{-1}), indicating denser crosslinks and firmer structures. In conclusion, KGM improved the texture and viscoelasticity of PFB and had an excellent application value in developing plant-based seafood analogues.

1. Introduction

Seafood has been suggested as a part of a balanced diet due to its high-quality nutrients (FAO & WHO, 2011) and positive health impact (Willett et al., 2019). Global seafood consumption has been significantly elevated because of rapid population growth and the rise of aquaculture over the past 50 years (Marwaha et al., 2020). The rising seafood consumption prompts marine farming of seafood and its production, resulting in overfishing, dwindling of marine biodiversity, environmental destruction, and fish disease (Almeida, Karadzic, & Vaz, 2015). Furthermore, seafood consumption increases the risk of allergy, toxic substances intakes, such as heavy metals (mercury) and ciguatoxins (Mahaffey et al., 2011). These concerns and the shift towards vegetarian dietary habits encourage the development of plant-based seafood substitutes, imitating the texture and sensorial characteristics of seafood or processed fish products (Kazir & Livney, 2021). Plant-based seafood is seeing elevating investment, which could help to reduce pressure on pressure on global fisheries. Upward of 20 well-established food manufactures, including Gardein, Good Catch Foods, New Wave Foods, Amazon, and Tesco (Kazir & Livney, 2021), are working on alternative seafood imitating shrimp, tuna, fish burgers.

The texture of seafood products is characterized by elasticity and breakdown sensation during mastication. Mimicking the texture is critical for the overall quality and acceptability of seafood substitutes by consumers. However, most companies aim to imitate the appearance, smell, and flavoring of seafood rather than mimic the structure and texture attributes. Extrusion cooking is a widely used technology in meat analog production (McHugh & Avena-Bustillos, 2019; Yuliarti, Kovis, & Yi, 2021), whereas it increases the processing cost and makes final products more expensive. Another alternative technique to mimicking seafood texture is binding plant proteins with polysaccharides. For instance, alginates can form strong polysaccharide gels entrapping proteins. Microbial transglutaminase makes proteins crosslinked to create robust gel networks (Moreno, Carballo, & Borderías, 2008).

Konjac glucomannan (KGM) is a water-soluble polysaccharide extracted from konjac (*Amorphophallus konjac*) tubers. It has been increasingly used as a food additive or food supplement, considering its health benefits, such as preventing diabetes, obesity, and hyperglycemia

* Corresponding author at: Department of Food Science & Technology, National University of Singapore, Singapore 117542, Singapore.
E-mail address: fstynghs@nus.edu.sg (H. Yang).

https://doi.org/10.1016/j.ifset.2021.102910
Received 1 November 2021; Received in revised form 18 December 2021; Accepted 21 December 2021
Available online 24 December 2021

(Jiang, Reddy, Huang, Chen, & Xu, 2019). KGM is a random linear copolymer consisting of β-1, 4 linked D-glucose and D-mannose in a molar ratio of 1: 1.6 (Jiang et al., 2019), with a side chain containing acetyl groups (5–10%). The acetyl groups in native KGM molecules could prevent them from associating with each other. Under alkaline conditions, deacetylation replaces the acetyl groups with hydroxyl groups and generates deacetylated KGM (Yang et al., 2017). The deacetylated KGM can form self-aggregation and polymer chain association through hydrogen bonding. The deacetylation and concentration are critical for KGM to create a thermal irreversible elastic gel (Solo-de-Zaldívar, Tovar, Borderías, & Herranz, 2014).

Furthermore, KGM has been authorized as GRAS (Generally Recognized as Safe) (Jimenez-Colmenero, Cofrades, Herrero, Solas, & Ruiz-Capillas, 2013) and used as a food additive in European countries. For instance, KGM was employed as a fat-replacer to produce low-fat mayonnaise, skimmed yogurt, and cheese (da Silva, de Souza Ferreira, Bruschi, Britten, & Matumoto-Pintro, 2016; Xu et al., 2020), suggesting that KGM improved the texture, rheological properties, and storage stability of these products. KGM was also used to prepare low-fat frankfurters, restructured gilthead sea bream, restructured pork nuggets, and low-fat sausages (Jiménez-Colmenero et al., 2012). Their water holding capacity, chewiness, cohesiveness, and gel strength were significantly enhanced by the addition of KGM.

To the best of our knowledge, little research is accessible concerning the application of KGM in developing plant-based seafood analogues and its effects on the texture and rheology of seafood substitutes. In addition, fishball (FB) is a processed fish product prepared from minced fish meat or fish surimi, with or without starch, flavor enhancer, and food conditioner (Tee & Siow, 2014). FB is gaining great popularity in countries like Australia, Japan, the U.S., China, and Southeast Asian countries (Tee & Siow, 2014). Therefore, this study took FB as an example of processed seafood products and applied KGM in developing plant-based fishball (PFB) substitutes. Our preliminary experiments showed that adding KGM (5.0%) to SPI could generate a PFB with a gel-like and chewy texture. The objective is to mimic the unique texture of FB counterpart and investigate the effects of KGM on the physico-chemical, textural, and rheological characteristics of PFB; to demonstrate the application value of KGM in plant-based seafood analogues mimicking texture of seafood products.

2. Materials and methods

2.1. Materials

Soy protein isolate (SPI) was purchased from Myprotein (Cheshire, UK), containing 90.0% protein, 1.5% fat, and 1.8% carbohydrate. KGM powder was purchased from iHerb (Moreno Valley, CA, USA). Dietary alkali (sodium carbonate), sea salt, tapioca starch, sucrose, and sunflower oil were purchased from a local supermarket in Singapore. Frozen fish surimi (*Big eye*, *Itoyori*, and *Leather jacket*) was provided by Thong Siek Food Industry Pte Ltd. (Singapore).

2.2. Sample preparation

Based on preliminary experiments, the concentration of SPI was fixed at 7.0% (*w*/w). The SPI was hydrated with 30% deionized water for 30 min. Sea salt (1.5%, w/w), sunflower oil (3.5%, *v/w*), sucrose (0.5%, w/w), and dietary alkali (0.5%, w/w) were then added. Moreover, ice (49.5–53.5%, w/w) was used to make up the weight difference and prevent heat generation during stirring. The mixture was blended for 5 min using a food processor (Panasonic, Osaka, Japan). Afterward, different levels of KGM (up to 8.0%, w/w) were slowly added into the food processor while blending. The raw PFB mixtures with different KGM concentrations were obtained (the pH for PFB3.5, PFB5.0, PFB6.5, and PFB8.0 paste were 10.01 ± 0.54, 9.97 ± 0.81, 9.98 ± 0.41, and 9.91 ± 0.70, respectively). Part of the mixture (around 20 g) was taken out immediately for rheological measurements. The remaining part was manually made into PFB (30.0 ± 1.0 g), which were put in aluminum foil bowls (15.24 cm in diameter, three fishballs per bowl), and then steamed in water bath at 90 °C for 30 min. The deacetylation degree of mixtures containing KGM after cooking was measured based on the description of Hu et al. (2019). The deacetylation degree for mixtures with 3.5%, 5.0%, 6.5%, and 8.0% were 35.6%, 47.8%, 61.1%, and 73.6%, respectively. The remained cooked samples were stored overnight in a fridge at 4 °C before measurements.

For FB preparation, frozen fish surimi was thawed overnight at 4 °C before use. FB was prepared as follows: Frozen surimi (88.5%, *w*/w), tapioca starch (5.0%, w/w), sea salt (1.5%, w/w), and deionized water (5.0%, *v/w*) were blended for 5 min. The following procedures were carried out in the same way with PFB samples. BFB (fishball made from *Big eye* surimi), IFB (fishball made from *Itoyori* surimi), and LFB (fishball made from *Leather jacket* surimi) were prepared to conduct texture profile analysis (TPA) using a texture analyzer.

2.3. Proximate composition and physical properties

The proximate composition, including moisture, protein, total fat, and total ash, was evaluated using the AOAC (2005) standard methods.

Expressible moisture was determined as described in a previous study (Zhou & Yang, 2019). The sample (about 2 g) was put between three filter papers (two at the bottom and one on the top) and subjected to a weight of 5 kg for 2 min. The expressible moisture (%) was calculated as follows:

$$\text{Expressible moisture} = \left(\frac{\text{weight before compression} - \text{weight after compression}}{\text{weight before compression}}\right) \times 100\% \quad (1)$$

The cooking yield of samples was determined based on the weight before and after cooking (Shin, Lee, Lee, Jo, & Choe, 2020):

$$\text{Cooking yield } (\%) = \frac{\text{Sample weight after cooking (g)}}{\text{Sample weight before cooking (g)}} \times 100\% \quad (2)$$

Moreover, the pH values of FB and PFB were also determined using a pH meter (FiveEasy Plus pH meter FP20, Mettler Toledo, USA).

2.4. Texture profile analysis

Samples were cut from the center of the fishball into cubes of 15 mm (Feng et al., 2020). The texture profile analysis was conducted using a texture analyzer (TA.XT2i Texture Analyzer, Stable Micro Systems Co. Ltd., Godalming, UK). The test speed was 1 mm/s, and the compression distance was 6 mm (40% of the sample height). Textural parameters, including hardness, cohesiveness, springiness, chewiness, and resilience, were determined.

2.5. Rheological measurements

Food texture attributes are generally correlated to the rheological

properties of food materials (Do Trong et al., 2014). The rheological behavior of FB and PFB was performed on a rotational stress-controlled rheometer equipped with Anton Paar MCR 102 (Anton Paar, Graz, Austria). A parallel stainless-steel plate with a diameter of 25 mm was applied, with a gap between the sample holder and plate fixed at 1.0 mm. A strain sweep was firstly conducted at 25 °C, with an angular frequency of 62.83 rad/s, an initial strain of 0.01%, a final strain of 100%, and a point number of 25, to determine the linear viscoelastic range (LVER) and gel characteristics in this range. The LVER could help to pre-set a consistent strain and stress value for further measurements. Afterward, frequency sweep and creep-recovery tests were performed to characterize viscoelastic properties.

At the gel state, a frequency sweep (100–0.1 rad/s) was performed at 25 °C with a fixed strain amplitude γ of 0.5%, ensuring the test was conducted within the LVER (Yang, Gao, & Yang, 2020). Silicone oil was used to seal the sample to prevent evaporation. A mechanical spectrum was obtained after the measurement, and the storage modulus G′, loss modulus G″, and complex viscosity (η*) were obtained. A power-law function was used to fit the data as follows (Iglesias-Otero, Borderías, & Tovar, 2010; Xiong et al., 2019):

$$G' = G'_0 \bullet \omega^{n'} \tag{3}$$

$$G'' = G''_0 \bullet \omega^{n''} \tag{4}$$

$$\eta^* = K_f \bullet \omega^{-n_f} \tag{5}$$

G'_0 and G''_0 indicate the elastic moduli and viscous moduli at a frequency of 1 rad/s respectively; n′, n″ indicate the changing rate of G′ and G″ with ω. Moreover, K_f is a dynamic consistency index that shows the interaction strength, and n_f is a dynamic power-law factor that shows the extent of network extension.

A creep-recovery test was performed at the gel state to further understand the textural characteristics of FB and PFB using the same rheometer. At the creep phase, constant shear stress of 150 Pa was used from 0 to 373.5 s. The stress was then removed, after which the variations in strain were recorded from 373.5 to 747 s (recovery stage). A Burgers model was applied to fit compliance J (t) data (Zhuang, Wang, Jiang, Chen, & Zhou, 2021). Furthermore, the percent recovery R% (elasticity) during the test was calculated based on Jmin and Jmax (Herranz, Tovar, Solo-de-Zaldívar, & Borderias, 2012).

$$J(t) = J_0 + J_1 \bullet [1 - \exp(-t/\lambda_1)] + t/\eta_0 \tag{6}$$

$$R(\%) = \frac{J_{max} - J_{min}}{J_{max}} \times 100 \tag{7}$$

J (t) indicates the compliance during creep recovery test at time t; J_0 and J_1 indicate instantaneous elastic and retarded elastic compliance, respectively; J_{max} and J_{min} indicate maximum compliance J (the end of creep step) and minimum compliance J (the end of the recovery step), respectively; η_0 is the zero-shear viscosity of samples.

In addition, relaxation modulus G (t) data, provided by the rheometer during creep time, were also fitted as follows (Herranz, Tovar, Borderias, & Moreno, 2013). The equation served to derive material-characteristic parameters, gel strength (*S*) and relaxation exponent (*n*) (Moreno et al., 2020):

$$G(t) = S \bullet t^{-n} \tag{8}$$

where *S* is determined as gel strength indicating properties of crosslinks within the gel networks in a transient test; *n* is relaxation exponent indicating temporal dependence of the crosslinks within the networks (Herranz et al., 2013).

The goodness-of-fit was expressed as R^2, RMSE (Root Mean Squared Error), SSE (Sum of Squares Error), and SSR (Sum of Squares due to Regression), which were determined as follows:

$$RMSE = \sqrt{\frac{\sum_{i=1}^{N}(y_i - \hat{y}_i)^2}{N}} \tag{9}$$

$$SSE = \sum_{i=1}^{N}(y_i - \hat{y}_i)^2 \tag{10}$$

$$SSR = \sum_{i=1}^{N}(\hat{y}_i - \bar{y}_i)^2 \tag{11}$$

where parameter *i* is a variable, *N* is the total number of values, y_i represents observed value, $\hat{y}_i$ is the estimated value, $\bar{y}_i$ represents mean value.

2.6. Microstructure

The microstructure of PFB and FB was analyzed using a Quanta-250 scanning electron microscope SEM (FEI Co., Hillsboro, USA). Freeze-dried PFB and FB were sprayed onto aluminum plates and coated with a thin layer of gold. The samples were then visualized under the microscope with an acceleration voltage of 15 kV and SPS.

2.7. Secondary structure determination

The secondary structures of FB and PFB were determined through a Fourier Transform Infrared Spectroscopy FTIR (PerkinElmer, MA, USA), with a scan range from 4000 to 450 cm^{-1}, a resolution of 4 cm^{-1}, and a scan number of 32 (Yang, Yang, & Yang, 2018). Samples were firstly lyophilized and ground with KBr in a ratio of 1: 50. Full-band scanning was conducted with KBr as a blank before each test. The spectra were processed via OMNIC 8.0 (Thermo Fisher Scientific, Waltham, MA, USA) and Peak Fit v4.12 (Systat Software, Inc., San Jose, CA, USA). Baseline correction and Fourier self-deconvolution were conducted, followed by second-order derivation and Gaussian curve fitting. Each protein secondary structure content was determined by the peak area of each protein structure component divided by the amide I region's overall peak area (1600–1700 cm^{-1}) after the analysis.

2.8. Statistical analysis

Experimental results were processed through SPSS software (IBM Corp., Armonk, NY, USA) and presented as mean values ± the standard deviation. The statistical difference within and among sample groups was evaluated through a one-way analysis of variance (ANOVA). At least three repetitions were conducted for each test. Significant statistical differences presented when *P*-value < 0.05.

3. Results and discussions

The overall appearance and cutting profiles of FB and PFB are shown in Fig. S1, which showed that PFB with less than 3.5% of KGM could not form a solid-like gel and fishball shape (Fig. S1D - F). Therefore, more than 3.5% of KGM was added to prepare PFB. The texture, rheological, and physicochemical characteristics of PFB were studied. Generally, the overall appearance of PFB3.5, PFB5.0, PFB6.5, and PFB8.0 was like FB. However, from the cutting profiles, the inside texture of FB was compact with uniformly distributed and small pores, while PFB3.5 had a soft and loose texture with the most prominent pores. With the increasing KGM level, PFB had fewer and smaller pores, which made the inside texture of PFB more compact and denser. These pores in PFB could be formed during the blending process when the air was caught into the water. KGM has a great water-binding capacity, which could decrease bubble formation in PFB with higher KGM concentrations. The inside texture of PFB8.0 was highly tight, possessing the smallest pores, while PFB6.5 had a similar inside texture to IFB.

3.1. Proximate compositions and physical properties

The moisture content of FB ranged from 71.78 to 73.86%, whereas that of PFB ranged from 78.64 to 80.76%. The protein content of FB prepared in our study was 11.13 to 14.01%, while PFB had a much lower protein content (5.89 to 6.09%) compared with IFB. Nonetheless, a previous study has reported that the protein content of commercial fishball was from 7.54 to 9.89% (Huda, Shen, Huey, & Dewi, 2010), which had closer protein content to PFB prepared in this study.

The pH values of PFBs decreased from 9.38 to 7.93, with increased KGM from 3.5 to 8.0% (Table S1). The deacetylation of KGM under alkali conditions involves replacing acetyl groups with hydroxyl groups (Yang et al., 2017). Before cooking, the pH of the PFB mixtures with different KGM concentrations was around 10.0 without a significant difference. During heating (under alkaline conditions), PFB mixtures containing higher KGM concentration showed a higher deacetylation degree (increased from 35.6 to 73.6%), leading to a more decrease of alkalinity and free hydroxyl ions [OH^-]. Therefore, the pH decreased more after cooking in PFB with a higher KGM addition.

Expressible moisture and cooking yield could reflect water-holding capacity. The lower expressible moisture and cooking loss reveals the higher water-holding capacity. As indicated in Table S1, no significant difference in expressible moisture and cooking yield was found among FBs. For PFB, as KGM addition increased from 3.5 to 8.0%, the expressible moisture decreased significantly from 7.24 to 2.57%. In comparison, the cooking yield increased from 96.96 to 99.34%, indicating that KGM improved the water-holding capacity and cooking quality of PFB. This was because KGM has a great water-binding capacity and can absorb a large volume of moisture (Zhuang et al., 2021). More free water was changed to bound water, which could be trapped in the three-dimensional networks. Consequently, the water-holding capacity was improved, and cooking loss was reduced. PFB6.5 showed an insignificant difference in expressible moisture with IFB (3.20% for PFB6.5, and 3.97% for IFB, respectively), indicating that PFB6.5 had a close water-holding capacity to IFB.

3.2. Texture profile analysis

Textural parameters were determined, including hardness, gumminess, cohesiveness, springiness, resilience, and chewiness. As shown in Fig. 1A, the hardness of BFB, IFB, and LFB were 3467.17, 1852.56, and 2331.37 g, respectively. The result was consistent with the hardness of commercial fishball (1710–3010 g) (Huda et al., 2010). IFB had the lowest hardness compared with other FBs. For PFB, as KGM addition increased, the hardness increased significantly from 880.22 to 3629.61 g (Fig. 1A). The increase of hardness might be resulting from removing acetyl groups through deacetylation could make KGM transform from semi-crimping to self-crimping, leading to self-aggregation and the formation of three-dimensional networks that can trap water to form a rigid and compact structure (Wang et al., 2017). PFB6.5 had no significant difference in hardness (1957.31 g) with IFB (1852.56 g), whereas PFB8.0 had an excessive hardness (3629.61 g) compared with IFB and other PFBs.

There was no significant difference in cohesiveness and springiness between FB and PFB, except for PFB3.5 (Fig. S2A). PFB6.5 showed no significant difference in gumminess, resilience with IFB. However, the chewiness of PFB increased significantly with increasing KGM. The chewiness is the energy necessary to chew a solid food to a status that is ready to swallow (Liu, Xu, & Guo, 2008), which is an essential indicator of mouthfeel (Varela, Mosca, Nguyen, McEwan, & Berget, 2021). The chewiness of PFB was incredibly enhanced by KGM from 561.93 to 2787.54 g·mm (Fig. 1B), demonstrating that structural strength was enhanced in PFB6.5 and PFB8.0. The increased chewiness by KGM might be explained by the long-chain polysaccharide effect that could connect the entire protein network and strengthen the composite gel structure. Previous studies have suggested that KGM could significantly enhance

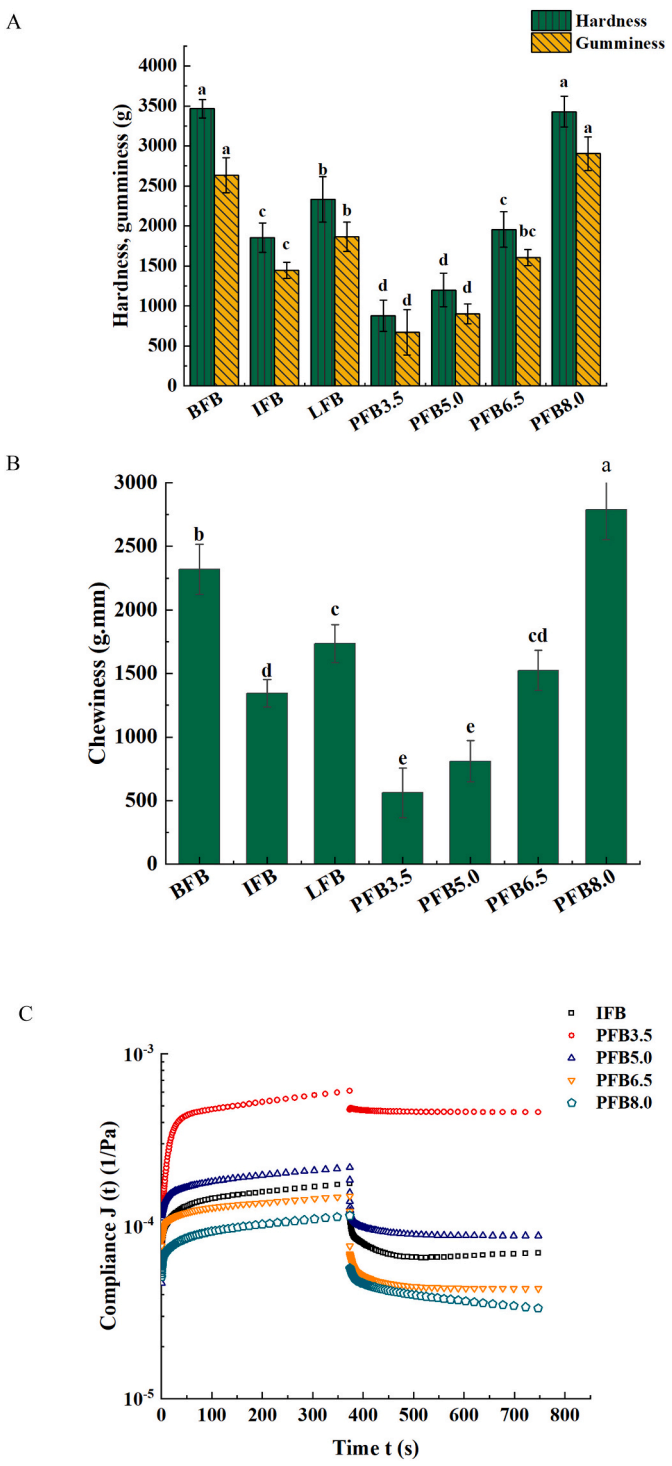

Fig. 1. The hardness and gumminess (A); the chewiness (B); the creep-recovery plots of creep compliance changes with time (C) of fishball and plant-based fishball analogue.

the compression force and texture attributes of restructured meat (Iglesias-Otero et al., 2010; Xiong et al., 2009). There was no significant difference in chewiness between IFB and PFB6.5. However, PFB8.0 had a significantly higher chewiness than other PFBs and IFB, making PFB8.0 harder to swallow.

The texture is a critical and direct factor that affects consumer acceptance. IFB exhibited a lower hardness, gumminess, and chewiness, which was more acceptable of fishball. Therefore, IFB was selected as a control group for the subsequent rheological and microstructural

analysis. Overall, the TPA results showed that KGM addition was suggested to be 6.5% (PFB6.5), considering the hardness, gumminess, and chewiness. More than 6.5% KGM addition (PFB8.0) could lead to a rigid and chewy texture.

Although texture profile analysis can provide helpful sensory perception and quality control information, this empirical measurement depends on test conditions and cannot provide true material parameters. Meantime, small deformation oscillatory tests provide critical information correlated to the network structure of food gels, presenting complex viscoelastic performance (Herranz et al., 2012). Therefore, a thorough rheological measurement is essential to determine the true mechanical and structural parameters.

3.3. Rheological properties

3.3.1. Determination of linear viscoelastic region

A strain sweep was firstly conducted to determine the LVER, where storage modulus (G′) and loss modulus (G″) is not dependent on shear strain, which could guarantee a sample's inner structure integrity (Liu et al., 2018; Moreno et al., 2020). As shown in Fig. S2B, the LVER became broader with increasing KGM, indicating a better network coupling, demonstrating that KGM improved the gel quality of PFB.

3.3.2. Determination of viscoelastic properties

In a frequency sweep test, mechanical spectra can be expressed as a function between G′, G″, and the angular frequency (Iglesias-Otero et al., 2010). The plotting of G′ and G″ (Fig.S2C) was properly fitted with power-law function (Eqs. (3) and (4)), with $R^2 > 0.90$, RMSE < 0.04, SSE < 0.04 and $R^2 > 0.94$, RMSE < 0.06 SSE < 0.10, respectively (Table 1). G'_0 and G''_0 of PFBs (corresponding to the elastic and viscous resistance to gel deformation at 1 rad/s) were significantly increased with increasing KGM, indicating a larger gel firmness and rigidity. The increase of G'_0 in PFB at higher content of KGM demonstrated that more compact structures and networks were formed, and thus more energy was stored during shearing. There was no significant difference in G'_0 and G''_0 between IFB (589 kPa in G'_0, 85.4 kPa in G''_0) and PFB6.5 (579 kPa in G'_0, 88.9 kPa in G''_0).

Since the decreasing rate of G″ value with decreased frequency was higher than that of G′ (n″ > n′) for PFB3.5 sample, loss factor tan δ (G″/G′) decreased with decreasing frequency (Fig.S2D), indicating a "shear-induced gelation" phenomenon in PFB3.5 (Piñeiro-Lago, Franco, & Tovar, 2020), a natural behavior existing in vegetal gels from legume proteins (Moreno et al., 2020). Besides, tan δ of PFB3.5 changed more rapidly with frequency than PFB with higher KGM concentration, reflecting that low KGM addition less stable gel networks and thus less gel-like characteristics irrespective of frequency (Piñeiro-Lago et al., 2020). In addition, the tan δ of PFB decreased when KGM increased from 5.0 to 8.0%, indicating an improvement of the viscoelasticity in PFB at higher KGM addition.

The power exponents n′ and n″ are critical parameters to determine the time-stability of gel network reflecting frequency dependence of G′ and G″ (Borderías et al., 2020). Compared with IFB, the overall n′ (except for PFB8.0) and n″ of PFB were significantly higher, indicating the G′ and G″ of PFB showed higher frequency-dependence and thus less time-stability. Furthermore, compared with IFB ($n' = 9.69 \times 10^{-2}$) and PFB3.5 ($n' = 11.15 \times 10^{-2}$), the n′ decreased significantly in PFB8.0 ($n' = 5.02 \times 10^{-2}$). At the same time, n″ exponents increased from 11.17×10^{-2} to 17.6×10^{-2} in PFB samples with KGM levels increased from 5.0 to 8.0%, reflecting the rate of decrease of G" with decreasing angular frequency is higher than that of G′. The phenomenon could be attributed to the existence of shear-induced gelation in PFB (Piñeiro-Lago et al., 2020).

The changes in complex viscosity η* throughout the frequency sweep region are shown in Fig. S2E. The complex viscosity η* measures overall resistance to flow, represented as the ratio of complex modulus G* to angular frequency ω (G*/ω) (Tunick, 2011). The results showed that the η* increased significantly with increasing KGM from 3.5 to 8.0% in PFB, reflecting that the overall resistance to flow (as a function of ω) increased in PFB with the increased KGM levels. PFB8.0 had the highest complex viscosity η* compared with IFB and other PFBs throughout the entire frequency range. Furthermore, the data were properly fitted with Eq. (5), with $R^2 > 0.90$, RMSE < 0.08, and SSE < 0.02 (Table 1). The power-law factor n_f ($0 < n_f < 1$) denotes the degree of viscous and elastic behavior. The system exhibits an absolute elasticity when the n_f value equals 1, while the system exhibits an absolute viscosity when n_f equals 0 (Sow, Nicole Chong, Liao, & Yang, 2018). As shown in Table 1, the n_f of PFB increased from 0.77 to 0.89 with increasing KGM, indicating that a higher addition of KGM (6.5% and 8.0%) improved the elastic behavior of PFB. PFB6.5 showed no significant difference in n_f with IFB, demonstrating that 6.5% of KGM lead PFB to a similar rheological and structural behavior as IFB. Besides, as shown in Table 1, the interaction strength (K_f) in the PFBs was also enhanced by KGM significantly (153 to 721 $kPa{\cdot}s^{-nf}$). The reason could be that PFB with higher KGM addition exhibited more numerous and larger junctions, leading to stronger interactions and denser crosslinks within the gel networks. Moreover, KGM could form an entangled network when combined with protein and thus enhance the interaction and extension strength (Iglesias-Otero et al., 2010). However, with too much KGM addition (8.0%) in PFB, a highly compact and denser crosslink could be formed, leading to a too hard and chewy texture compared with IFB and other PFBs.

Table 1
Fitting parameters of Eqs. (3), (4), and (5) from the power-law model for fishball and plant-based fishball analogue.

		IFB	PFB3.5	PFB5.0	PFB6.5	PFB8.0
Eq. (3)	G'_0 ($kPa{\cdot}S^{-n'}$)	589 ± 31^{b}	252 ± 21^{d}	347 ± 24^{c}	579 ± 31^{b}	912 ± 40^{a}
	n′ ($\times 10^{-2}$)	9.69 ± 0.26^{b}	11.15 ± 0.15^{a}	10.49 ± 0.63^{ab}	10.72 ± 0.14^{a}	5.02 ± 0.53^{c}
	R^2	0.98	0.99	0.91	0.89	0.96
	RMSE ($\times 10^{-2}$)	1.29	0.77	3.15	3.69	2.64
	SSE ($\times 10^{-2}$)	0.74	0.17	2.88	3.96	2.01
Eq. (4)	G''_0 ($kPa{\cdot}S^{-n''}$)	85.4 ± 7.2^{a}	43.4 ± 4.2^{b}	83.4 ± 9.0^{a}	88.9 ± 8.1^{a}	91.7 ± 9.4^{a}
	n″ ($\times 10^{-2}$)	8.89 ± 0.13^{d}	29.2 ± 1.3^{a}	11.17 ± 0.56^{c}	16.88 ± 0.74^{d}	17.6 ± 1.2^{b}
	R^2	0.99	0.99	0.94	0.95	0.95
	RMSE ($\times 10^{-2}$)	0.63	1.47	2.79	3.69	5.80
	SSE ($\times 10^{-2}$)	0.41	0.63	2.26	3.95	9.76
Eq. (5)	K_f ($kPa{\cdot}s^{-n_f}$)	256 ± 16^{c}	153 ± 11^{d}	248 ± 19^{c}	599 ± 31^{b}	721 ± 37^{a}
	n_f ($\times 10^{-2}$)	88.1 ± 2.7^{b}	77.2 ± 2.2^{c}	84.7 ± 2.3^{b}	88.8 ± 2.0^{b}	89.4 ± 2.5^{a}
	R^2	0.99	0.99	0.98	0.96	0.94
	RMSE ($\times 10^{-2}$)	1.10	0.74	5.48	5.22	8.36
	SSE ($\times 10^{-2}$)	0.35	0.16	8.72	7.90	20.30

*Different lowercase letters for same parameter mean significant difference (n = 3, $P < 0.05$).
*IFB represented fishball made from *Itoyori* surimi. PFB3.5, PFB5.0, PFB6.5, and PFB8.0 represented PFB with a KGM concentration of 3.5%, 5.0%, 6.5%, and 8.0%.
*RMSE indicates root mean square error; SSE indicates sum of squares error.

3.3.3. Determination of creep compliance

The creep compliance J(t) of samples was measured via a creep recovery test that involves a light deformation during rheological measurements and could determine further textural characteristics. The measurement of creep compliance could be used to compare and determine the structural characteristics of different materials on a larger time scale (Herranz et al., 2013). Generally, higher creep compliance indicates more sequential rupturing of crosslinks could occur during loading so that originally short molecular fragments having weaker crosslinks might rupture (Herranz et al., 2013). Chattong, Apichartsrangkoon, Chaikham, Supavititpatana, and Bell (2015) showed that a gel with higher elasticity and firmness exhibits a lower value of creep compliance. As shown in Fig. 1C, the compliance increased dramatically at the creep phase and then decreased slowly at the recovery phase for all samples. Overall, the J(t) of PFB decreased with increasing KGM concentration, which showed that KGM improved the strength of crosslinks within the gels. The creep curves were fitted with a Burgers model (Eq. (6)), showing a good fitting with $R^2 > 0.98$, RMSE $< 1.87 \times 10^{-6}$, and SSR $< 9.04 \times 10^{-8}$. Therefore, the Burgers model could describe the viscoelastic behaviors of IFB and PFB.

Previous studies have demonstrated that fitting parameters J_0 and J_1 negatively correlate with gel firmness (Chattong, Apichartsrangkoon, & Bell, 2007). Table 2 shows that J_0 and J_1 were decreased significantly with increasing KGM, demonstrating a firmer and compact network of PFB at a higher concentration of KGM. The deacetylation of KGM results in the formation of stiffened aggregation (Huang, Takahashi, Kobayashi, Kawase, & Nishinari, 2002). KGM with a higher concentration had a higher deacetylation degree (increased from 35.6 to 73.6%), leading to more stiffened molecular aggregations and thus firmer structure in PFB. Moreover, more hydrogen bonds, hydrophobic interaction, and denser crosslinks could be formed within the PFB gel network at a higher KGM addition, strengthening the deformation resistance. There was no significant difference in J_0 between PFB6.5 (77.3×10^{-6} Pa^{-1}) and IFB (74.8×10^{-6} Pa^{-1}), which was consistent with TPA results that PFB had similar hardness with IFB (Table 2). However, PFB8.0 had a significantly lower J_0 (58.1×10^{-6} Pa^{-1}) than IFB, which could be attributed to a highly compact and dense structure formed in the PFB8.0 gel network. These results were consistent with the TPA results that showed the hardness and chewiness of PFB6.5 were closer to IFB, while PFB8.0 had a too hard and chewy texture compared with IFB.

Meantime, η_0 means the resistance required to make a viscoelastic material flow. A higher η_0 indicates a more considerable flow resistance and thus more solid-like attributes (Chattong et al., 2007). As shown in Table 2, η_0 increased in PFB with a higher level of KGM, indicating PFB with a higher KGM addition became more solid-like, while PFB3.5 showed less solid-like behavior than IFB and other PFB samples. Besides, retardation time λ denotes the time necessary for the postponed strain to 63.2% of the last value (Steffe, 1996). Samples with a longer retardation time achieve full deformation slowly. The λ of PFB showed a decreasing trend with increasing KGM, where PFB6.5 and PFB8.0 had lower λ value with 12.56 s and 12.1 s, respectively. In addition, the percent recovery R % (elasticity) of PFBs increased significantly from 24.7 to 70.9% when KGM increased from 3.5 to 8.0% (Table 2). PFB3.5 had the lowest elasticity (24.7%) compared with IFB and other PFBs. The reason could be that the concentration of KGM could affect the deacetylation rate and thus influence gelation speed in KGM/SPI system. Since PFB3.5 (with 3.5% of KGM) had lower viscosity, the KGM in PFB3.5 could be easier accessible to proceed with deacetylation (rapid gelation speed). Huang et al. (2002) indicated that rapid gelation would result in sparse and inhomogeneous gels, while slow gelation would produce more homogeneous gels. Slow gelation also allows molecular chains to be incorporated as elastically active chains. Zhuang et al. (2021) suggested that a strengthened structure could also result in a higher R%. Therefore, incorporating KGM into PFB increased the elasticity of PFBs significantly. The elasticity of PFB6.5 (65.9%) did not differ significantly from IFB (62.6%).

3.4. Microstructure

The microstructures of IFB and PFB were visualized via SEM, and the images are shown in Fig. 2. The microstructures indicated that all samples had a network structure, which allowed the gels to exhibit a particular elastic characteristic. During heating, the protein chains unfolded and then aggregated, which led to a three-dimensional network. IFB possessed small and regularly distributed pores (indicated by yellow arrows) within the gel network (Fig. 2A), contributing to a compact and regular gel structure. For PFB samples, the network structures varied with the different concentrations of KGM. PFB3.5 possessed large and irregular pores, which led to a loose and soft structure. With increasing KGM addition, the pores decreased in size and were distributed more regularly, making the PFB gels more compact and intensive. This phenomenon might be because KGM could interact with SPI mainly through hydrogen bonds and thereby fill the pores of the SPI network, making the structure tighter and more compact. The decrease in pore size could also be explained by the long-chain polysaccharide effect that affected expanded protein aggregation and bonding, connecting the entire protein and thus strengthening the composite gel structures (Zhang, Xue, Li, Wang, & Xue, 2015). Zhang et al. (2015) indicated that KGM affected the pore size and roughness in the morphology of KGM- *Alaska Pollock* composite gels, making the gel compact and smooth. PFB6.5 had a compact network with tiny pores and a stable surface, which showed a generally similar microstructure to IFB. However, PFB8.0 had a highly compact network compared with IFB and other PFBs, which agreed with the results of the rheological analysis mentioned before. Moreover, the tan δ (G''_0/G'_0) of PFB8.0 was 0.10, which was lower than that of IFB (0.14) and other PFBs (0.15–0.24), also reflecting a highly compact network in PFB8.0 compared with IFB.

3.5. Schematic model

Based on the abovementioned discussions, we proposed a possible schematic model for PFB and FB texture formation representing interaction-structure-properties (Fig. 3). SPI chain is considered as a polymer of peptides containing various amino acids. KGM is a polysaccharide made up of D-glucose and D-mannose linked via β-1, 4 linkages, with a side chain containing acetyl groups (Fig. 3). Hydroxy groups can replace these acetyl groups through deacetylation under an alkaline condition, which was necessary to form a stable KGM gel

Table 2
The creep fitting parameters from the Burgers model for fishball and plant-based fishball analogue.

Sample	J_0 ($\times 10^{-6}$ Pa^{-1})	J_1 ($\times 10^{-6}$ Pa^{-1})	λ_1 (s)	η_0 ($\times 10^6$ Pa·s)	R^2	RMSE ($\times 10^{-6}$)	SSR ($\times 10^{-8}$)	R%
IFB	74.8 ± 5.8^{d}	53.5 ± 4.3^{c}	16.5 ± 1.0^{b}	7.24 ± 0.29^{c}	0.99	3.03	7.69	62.6 ± 1.2^{ab}
PFB3.5	101.3 ± 7.2^{a}	349 ± 13^{a}	30.0 ± 1.5^{a}	2.24 ± 0.08^{e}	0.99	8.17	2.23	24.7 ± 1.4^{d}
PFB5.0	88.9 ± 3.5^{b}	67.1 ± 4.6^{b}	14.05 ± 0.52^{c}	5.25 ± 0.31^{d}	0.98	8.20	9.04	56.5 ± 1.1^{c}
PFB6.5	77.3 ± 4.8^{cd}	44.5 ± 3.0^{c}	12.56 ± 0.77^{cd}	11.99 ± 0.64^{b}	0.98	2.59	2.95	65.9 ± 1.0^{b}
PFB8.0	58.1 ± 4.5^{a}	24.8 ± 2.8^{d}	12.1 ± 1.2^{d}	12.97 ± 0.41^{a}	0.98	1.87	2.24	70.9 ± 1.3^{a}

*Different lowercase letters for same parameter mean significant difference ($n = 3$, $P < 0.05$).
*IFB represented fishball made from *Itoyori* surimi. PFB3.5, PFB5.0, PFB6.5, and PFB8.0 represented PFB with a KGM concentration of 3.5%, 5.0%, 6.5%, and 8.0%.
*RMSE indicates root mean square error, SSR indicates sum of squares due to regression; R% indicates percent recovery in creep recovery test.

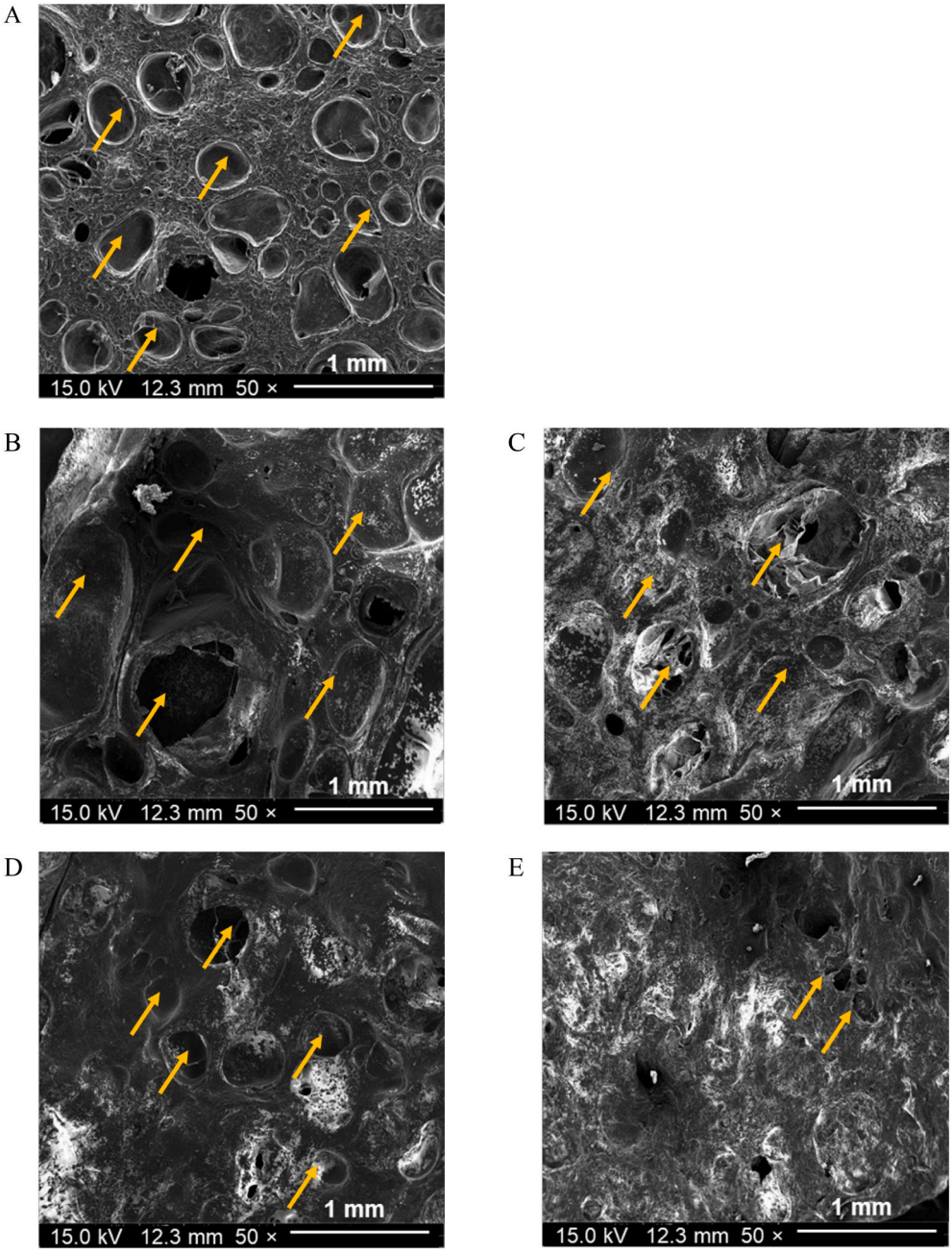

Fig. 2. The scanning electron microscope (SEM) images: (A), IFB (fishball made from *Itoyori* surimi); (B), PFB3.5 (plant-based fishball analogue with 3.5% of KGM); (C), PFB5.0 (plant-based fishball analogue with 5.0% of KGM); (D), PFB6.5 (plant-based fishball analogue with 6.5% of KGM); and (E), PFB8.0 (plant-based fishball analogue with 8.0% of KGM).

matrix. Wang, Yao, Jian, Sun, and Pang (2010) suggested that the SPI/KGM complex gel interactions were located at -OH groups of KGM mannose and glucose and the amide groups of SPI.

Moreover, the hydrogen bonds between KGM and SPI were primarily formed via a water bridge. Water was firstly distributed in SPI structures in the form of bound moisture and free moisture. Upon increasing KGM addition, more water within the gels was transformed to bound water, which was attributed to the excellent water-binding capacity of KGM.

Upon mixing SPI with KGM, the texture of PFB varied with KGM addition, which was resulted from different interactions between SPI and KGM. At a lower KGM addition (< 6.5%), weak hydrogen bonds and interactions result in a loose gel network. The loose gel network led to a final soft texture in PFB3.5 and PFB5.0, with a low hardness and gel strength. With the KGM addition increased to 6.5% (deacetylation degree 61.1%), more acetyl groups were replaced with -OH groups. More KGM junction zones formed, entrapping SPI chains and contributing to a more compact gel network and denser crosslinks. The flow resistance n_f and interaction strength K_f of PFB increased with increasing KGM, contributing to a more elastic property and stronger gel networks. Overall, the hardness and gel strength of PFB were progressively improved by KGM addition. PFB6.5 exhibited a matched texture with fishball (a compact gel network primarily formed through myosin denaturation and aggregation) (Fig. 3). However, with too much KGM addition (8.0%), PFB had a highly tough and chewy texture (hardness 3429.61 g and chewiness 2787.54 g·mm). The reason could be that the deacetylation degree increased significantly from 35.6 to 73.6% when the KGM level increased from 3.5 to 8.0%, forming more significant junctions and highly packed crosslinks in the SPI/KGM system.

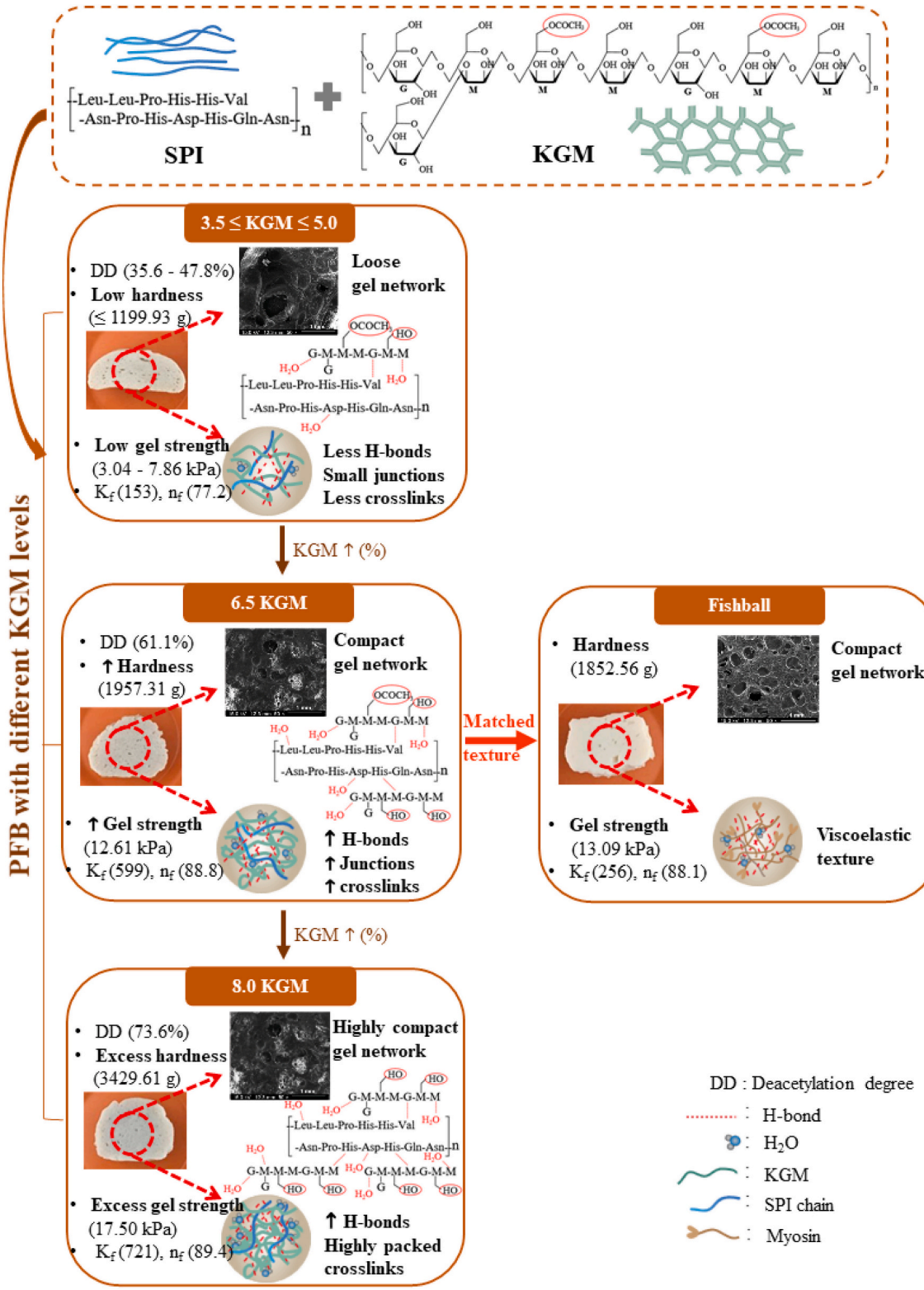

Fig. 3. The schematic model of the plant-based fishball analogue (PFB) and fishball (FB).

3.6. Validation of the schematic model

3.6.1. Validation by secondary structures

The conformational variation of PFB gel was investigated using FTIR to validate the schematic model. The deconvolution of amide I (1600–1700 cm^{-1}) could provide critical information about secondary structures presented as α-helix, β-sheet, β-turn, and random coil (Martínez et al., 2017). As shown in Table 3, compared with PFB0 (no KGM), PFB samples with KGM exhibited a higher percentage of α- helix and β-sheet but a lower percentage of β-turns and random coils. Moreover, the β-sheet was the main secondary component in PFB samples. This was because, at higher KGM addition, more hydroxyl groups were exposed, leading KGM to provide highly entangled networks surrounding SPI, which slowed down heat exchange during heating and made

Table 3
The characteristics of secondary structures for fishball and plant-based fishball analogue.

Sample	α-Helix (%)	β-Sheet (%)	β-Turn (%)	Random coil (%)	Helix/coil (%)
IFB	29.6 ± 1.2 ^{a}	31.5 ± 1.1 ^{d}	20.1 ± 1.1 ^{a}	18.8 ± 1.2 ^{ab}	1.57 ± 0.03 ^{bc}
PFB0	28.4 ± 1.0 ^{a}	32.7 ± 1.0 ^{cd}	17.92 ± 0.58 ^{bc}	20.90 ± 0.69 ^{a}	1.41 ± 0.01 ^{d}
PFB3.5	28.4 ± 1.2 ^{a}	34.1 ± 0.7 ^{bc}	17.1 ± 1.0 ^{cd}	20.4 ± 1.0 ^{a}	1.40 ± 0.03 ^{d}
PFB5.0	28.83 ± 0.88 ^{a}	35.05 ± 0.78 ^{ab}	16.94 ± 0.79 ^{cd}	19.2 ± 1.0 ^{ab}	1.50 ± 0.04 ^{c}
PFB6.5	29.67 ± 0.91 ^{a}	35.14 ± 0.94 ^{ab}	16.5 ± 1.0 ^{cd}	18.7 ± 1.1 ^{ab}	1.58 ± 0.05 ^{b}
PFB8.0	29.84 ± 0.94 ^{a}	36.28 ± 0.83 ^{a}	16.27 ± 0.89 ^{d}	17.61 ± 0.93 ^{b}	1.70 ± 0.06 ^{a}

*Different lowercase letters for same parameter mean significant difference (n = 3, $P < 0.05$).
*IFB represented fishball made from *Itoyori* surimi. PFB0 represented the sample without KGM. PFB3.5, PFB5.0, PFB6.5, and PFB8.0 represented PFB with a KGM concentration of 3.5%, 5.0%, 6.5%, and 8.0%.

protein detain more sheet structures.

As KGM addition increased in PFB, the contents of α- helix and β-sheet increased; however, the content of β-turns and random coils decreased. The α- helix structures are relevant to protein folding; thus, an increase in the α- helix content in PFB with a higher concentration of KGM might result from more interactions between SPI and KGM and the generation of a more compact gel structure. Furthermore, the transformation of β-turns to β-sheets demonstrated that more hydrogen bonds were formed in PFB at higher KGM levels, as β-sheet structures require more hydrogen bonds to bond with multiple hydrogens (Wang et al., 2017). Higher content of sheet structure results in a more organized gel matrix and higher gel strength. Similarly, Li, Qu, Feng, and Chen (2020) reported that increasing KGM concentrations enhanced the level of α-helix and β-sheet while decreasing β-turns and the random coils in wheat gluten. Meantime, they suggested that α-helix and β-sheet could improve secondary structure's stability and affect elasticity and firmness.

Additionally, the helix-to-coil ratio represents the triple helix content, and a low ratio of the helix to coil generally means a low content of triple helices (Sow, Kong, & Yang, 2018). As shown in Table 3, KGM enhanced the helix-to-coil ratio from 1.40 to 1.70, and the helix-to-coil of PFB6.5 (1.58) showed no significant difference with IFB (1.57). It was suggested that a low helix-to-coil ratio was relevant to the low hardness, chewiness, and gel strength of fish gelatin. The phenomenon could be because triple helices are regarded as junction zones in the formation of continuous and three-dimensional gel networks (Sow, Nicole Chong, et al., 2018). A higher concentration of KGM exposed more -OH groups, enhancing the physical entanglement effect and decreasing heat exchange, which could reduce the destruction of the intermolecular hydrogen bonds within PFB gel structures. These results further supported that a high level of KGM would diminish the denaturation of SPI and improve the gel functionality of PFB.

3.6.2. *Validation by gel strength and relaxation exponent*

Furthermore, fitting parameters *S* (representing gel strength) and *n* (relaxation exponent) were determined from Eq. (8). The parameters *S* and *n* in a transient test indicate crosslink properties of the gel networks and temporal dependence of the crosslinks, respectively. Generally, a higher *S* value indicates the formation of more significant junctions in KGM gel networks; at the same time, a lower exponent (*n*) indicates a higher degree of network connectivity and more time-stability of the gels (Moreno et al., 2020).

The specific values of fitting parameters (*S* and *n*) are summarized in Table S3. While increasing KGM addition in PFB from 3.5 to 8.0%, the gel strength (*S*) significantly improved from 3.04 to 17.50 kPa (Fig. 4 and Table S3). There was no significant difference in gel strength between PFB6.5 (12.61 kPa) and IFB (13.09 kPa). The enhanced gel strength for PFB could be explained by the increased deacetylation degree (35.6–73.6%) of increasing KGM (3.5–8.0%). With a higher deacetylation degree, more acetyl groups were replaced with hydroxyl groups, resulting in the formation of more junction zones (serving to entrap SPI chains) and thus forming packed structures (Solo-de-Zaldívar et al., 2014). Moreover, small junction zones tend to be formed in PFB having a low deacetylation degree (such as PFB3.5). These small junction zones could reduce inter-aggregate forces (Solo-de-Zaldívar et al., 2014), leading to a weak gel network. Wang et al. (2017) also reported that 5% KGM in wheat gluten could strengthen the gel structure by enhancing hydrophobic interactions between KGM and wheat gluten.

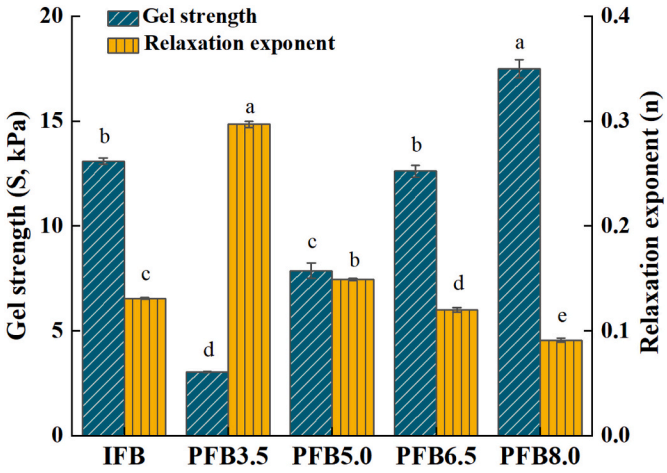

Fig. 4. The gel strength (S) and relaxation exponent (n) of fishball and plant-based fish ball.

Meantime, the relaxation exponent *n* decreased progressively (from 0.297 to 0.091) in PFB with increasing KGM concentration, indicating better network connectivity and stable crosslinks within the gel networks. The enhanced network connectivity (lower exponent *n* values in PFB6.5 and PFB8.0) could lead to a more hydrogen-bonded complex and thus a more compact structure. Besides, the physical entanglement effect of KGM would increase while increasing KGM concentration (Luo, He, & Lin, 2013), which would provide more stable molecular bonds (primarily hydrogen bonds) within SPI/KGM system.

Overall, with a higher KGM addition level, KGM chains were formed into more significant junctions (with high *S* values), increasing permanent crosslinks within networks (lower relaxation exponent *n*) (Solo-de-Zaldívar et al., 2014). PFB with too much KGM addition (8.0%) would form highly packed crosslinks within the gel networks.

4. Conclusion

The texture of PFB was significantly affected by KGM addition. The hardness, chewiness, and gel strength of PFB were improved significantly with increasing KGM. At a lower level of KGM (PFB3.5 and PFB5.0), the PFB had more and larger pores within the gel networks, resulting in a loose and weaker gel structure. No significant difference was found in gel strength, hardness, and microstructure between PFB6.5 and IFB.

The rheological behaviors were correlated with texture properties. With increasing KGM levels, PFB had higher elastic modulus G'_0 and consistency K_f, and lower instantaneous compliance J_0, consistent with texture profile analysis results. There was no significant difference in G'_0, n_f, and J_0 between PFB6.5 and IFB. The SEM images of PFBs supported the view that the gel structure became more compact with increasing KGM addition and that PFB6.5 had a matched structure while PFB8.0 had a highly compact structure. Additionally, the levels of α-

helices and β-sheets increased; simultaneously, β-turns and random coils were decreased at higher KGM concentrations, suggesting that KGM increased the elasticity and firmness of PFB. Furthermore, PFB with a higher level of KGM (PFB6.5 and PFB8.0) exhibited a higher helix-to-coil ratio, contributing to hardness, chewiness, and gel strength.

In conclusion, these findings indicated that KGM significantly improved the texture and rheological properties of PFB. Therefore, KGM had an excellent application value in developing plant-based seafood analogues as a critical contributor to mimicking the texture of seafood counterparts. By incorporating KGM with plant proteins, more varieties of plant-based seafood products could be developed mimicking the texture of seafood counterparts without using complicated high-pressure extrusion processing.

Declaration of Competing Interest

We declare that we do not have any commercial or associative interest that represents a conflict of interest connected with this manuscript. We have no financial and personal relationships with other people or organizations that can inappropriately influence our work.

Acknowledgments

The authors acknowledge the financial support by Applied Basic Research Project (Agricultural) Suzhou Science and Technology Planning Program (SNG2020061), Singapore Ministry of Education Academic Research Fund Tier 1 (R-160-000-A40-114), and an industry grant supported by Changzhou Wangxianglou Food Co., Ltd. (R-160-000-B22-597).

Appendix A. Supplementary data

Supplementary data to this article can be found online at https://doi.org/10.1016/j.ifset.2021.102910.

References

Almeida, C., Karadzic, V., & Vaz, S. (2015). The seafood market in Portugal: Driving forces and consequences. *Marine Policy, 61*, 87–94.

AOAC. (2005). *Official methods of analysis* (16th ed.). Washington, DC: Association of Official Analytical Chemists.

Borderías, A. J., Tovar, C. A., Domínguez-Timón, F., Díaz, M. T., Pedrosa, M. M., & Moreno, H. M. (2020). Characterization of healthier mixed surimi gels obtained through partial substitution of myofibrillar proteins by pea protein isolates. *Food Hydrocolloids, 107*, Article 105976.

Chattong, U., Apichartsrangkoon, A., & Bell, A. E. (2007). Effects of hydrocolloid addition and high pressure processing on the rheological properties and microstructure of a commercial ostrich meat product "Yor"(Thai sausage). *Meat Science, 76*(3), 548–554.

Chattong, U., Apichartsrangkoon, A., Chaikham, P., Supavititpatana, T., & Bell, A. E. (2015). Viscoelastic properties and physicochemical characteristics of pressurized ostrich-meat emulsions containing gum additives. *Innovative Food Science & Emerging Technologies, 32*, 64–69.

Do Trong, N. N., Rizzolo, A., Herremans, E., Vanoli, M., Cortellino, G., Erkinbaev, C., … Torricelli, A. (2014). Reprint of "Optical properties–microstructure–texture relationships of dried apple slices: Spatially resolved diffuse reflectance spectroscopy as a novel technique for analysis and process control". *Innovative Food Science & Emerging Technologies, 24*, 145–153.

FAO, & WHO. (2011). *Report of the joint FAO/WHO expert consultation on the risks and benefits of fish consumption, 25–29 January 2010*. Rome, Italy: World Health Organization.

Feng, X., Tjia, J. Y. Y., Zhou, Y., Liu, Q., Fu, C., & Yang, H. (2020). Effects of tocopherol nanoemulsion addition on fish sausage properties and fatty acid oxidation. *LWT - Food Science and Technology, 118*, Article 108737.

Herranz, B., Tovar, C. A., Borderias, A. J., & Moreno, H. M. (2013). Effect of high-pressure and/or microbial transglutaminase on physicochemical, rheological and microstructural properties of flying fish surimi. *Innovative Food Science & Emerging Technologies, 20*, 24–33.

Herranz, B., Tovar, C. A., Solo-de-Zaldívar, B., & Borderias, A. J. (2012). Effect of alkalis on konjac glucomannan gels for use as potential gelling agents in restructured seafood products. *Food Hydrocolloids, 27*(1), 145–153.

Hu, Y., Tian, J., Zou, J., Yuan, X., Li, J., Liang, H., Zhan, F., & Li, B. (2019). Partial removal of acetyl groups in konjac glucomannan significantly improved the rheological properties and texture of konjac glucomannan and kappa-carrageenan blends. *International Journal of Biological Macromolecules, 123*, 1165–1171.

Huang, L., Takahashi, R., Kobayashi, S., Kawase, T., & Nishinari, K. (2002). Gelation behavior of native and acetylated konjac glucomannan. *Biomacromolecules, 3*(6), 1296–1303.

Huda, N., Shen, Y. H., Huey, Y. L., & Dewi, R. S. (2010). Ingredients, proximate composition, colour and textural properties of commercial Malaysian fish balls. *Pakistan Journal of Nutrition, 9*(12), 1183–1186.

Iglesias-Otero, M. A., Borderías, J., & Tovar, C. A. (2010). Use of konjac glucomannan as additive to reinforce the gels from low-quality squid surimi. *Journal of Food Engineering, 101*(3), 281–288.

Jiang, Y., Reddy, C. K., Huang, K., Chen, L., & Xu, B. (2019). Hydrocolloidal properties of flaxseed gum/konjac glucomannan compound gel. *International Journal of Biological Macromolecules, 133*, 1156–1163.

Jiménez-Colmenero, F., Cofrades, S., Herrero, A. M., Fernández-Martín, F., Rodríguez-Salas, L., & Ruiz-Capillas, C. (2012). Konjac gel fat analogue for use in meat products: Comparison with pork fats. *Food Hydrocolloids, 26*(1), 63–72.

Jimenez-Colmenero, F., Cofrades, S., Herrero, A. M., Solas, M. T., & Ruiz-Capillas, C. (2013). Konjac gel for use as potential fat analogue for healthier meat product development: Effect of chilled and frozen storage. *Food Hydrocolloids, 30*(1), 351–357.

Kazir, M., & Livney, Y. D. (2021). Plant-based seafood analogs. *Molecules, 26*(6), 1559.

Li, S., Qu, Z., Feng, J., & Chen, Y. (2020). Improved physicochemical and structural properties of wheat gluten with konjac glucomannan. *Journal of Cereal Science, 95*, Article 103050.

Liu, H., Xu, X. M., & Guo, S. D. (2008). Comparison of full-fat and low-fat cheese analogues with or without pectin gel through microstructure, texture, rheology, thermal and sensory analysis. *International Journal of Food Science & Technology, 43*(9), 1581–1592.

Liu, Y., Liu, D., Wei, G., Ma, Y., Bhandari, B., & Zhou, P. (2018). 3D printed milk protein food simulant: Improving the printing performance of milk protein concentration by incorporating whey protein isolate. *Innovative Food Science & Emerging Technologies, 49*, 116–126.

Luo, X., He, P., & Lin, X. (2013). The mechanism of sodium hydroxide solution promoting the gelation of Konjac glucomannan (KGM). *Food Hydrocolloids, 30*(1), 92–99.

Mahaffey, K. R., Sunderland, E. M., Chan, H. M., Choi, A. L., Grandjean, P., Mariën, K., … Weihe, P. (2011). Balancing the benefits of n-3 polyunsaturated fatty acids and the risks of methylmercury exposure from fish consumption. *Nutrition Reviews, 69*(9), 493–508.

Martínez, M., Velazquez, G., Cando, D., Núñez-Flores, R., Borderías, A. J., & Moreno, H. (2017). Effects of high pressure processing on protein fractions of blue crab (Callinectes sapidus) meat. *Innovative Food Science & Emerging Technologies, 41*, 323–329.

Marwaha, N., Beveridge, M., Phillips, M., Komugisha, B., Notere Boso, D., Chan, C., Kabir, K., Sulser, T., & Wiebe, K. (2020). *Alternative seafood: Assessing food, nutrition and livelihood futures of plant-based and cell-based seafood*. Penang, Malaysia: WorldFish (Program Report: 2020-42).

McHugh, T., & Avena-Bustillos, R. (2019). How plant-based meat and seafood are processed. *Food Technology, 73*(10), 83–84 (87).

Moreno, H. M., Carballo, J., & Borderías, A. J. (2008). Influence of alginate and microbial transglutaminase as binding ingredients on restructured fish muscle processed at low temperature. *Journal of the Science of Food and Agriculture, 88*(9), 1529–1536.

Moreno, H. M., Domínguez-Timón, F., Díaz, M. T., Pedrosa, M. M., Borderías, A. J., & Tovar, C. A. (2020). Evaluation of gels made with different commercial pea protein isolate: Rheological, structural and functional properties. *Food Hydrocolloids, 99*, Article 105375.

Piñeiro-Lago, L., Franco, I., & Tovar, C. A. (2020). Temperature dependence of the viscoelastic properties of an acid-curd Spanish cheese: Afuega'l Pitu atroncau roxu variety (PDO). *LWT - Food Science and Technology, 126*, Article 109304.

Shin, D. J., Lee, H. J., Lee, D., Jo, C., & Choe, J. (2020). Fat replacement in chicken sausages manufactured with broiler and old laying hens by different vegetable oils. *Poultry Science, 99*(5), 2811–2818.

da Silva, D. F., de Souza Ferreira, S. B., Bruschi, M. L., Britten, M., & Matumoto-Pintro, P. T. (2016). Effect of commercial konjac glucomannan and konjac flours on textural, rheological and microstructural properties of low fat processed cheese. *Food Hydrocolloids, 60*, 308–316.

Solo-de-Zaldívar, B., Tovar, C., Borderías, A., & Herranz, B. (2014). Effect of deacetylation on the glucomannan gelation process for making restructured seafood products. *Food Hydrocolloids, 35*, 59–68.

Sow, L. C., Kong, K., & Yang, H. (2018). Structural modification of fish gelatin by the addition of gellan, kappa-carrageenan, and salts mimics the critical physicochemical properties of pork gelatin. *Journal of Food Science, 83*(5), 1280–1291.

Sow, L. C., Nicole Chong, J. M., Liao, Q. X., & Yang, H. (2018). Effects of κ-carrageenan on the structure and rheological properties of fish gelatin. *Journal of Food Engineering, 239*, 92–103.

Steffe, J. F. (1996). *Rheological methods in food process engineering*. Freeman Press.

Tee, E. T., & Siow, L. F. (2014). Physical and sensory properties of frozen Spanish Mackerel (*Scomberomorus guttatus*) fish balls added with cryoprotectants. *Food and Bioprocess Technology, 7*(12), 3442–3454.

Tunick, M. H. (2011). Small-strain dynamic rheology of food protein networks. *Journal of Agricultural and Food Chemistry, 59*(5), 1481–1486.

Varela, P., Mosca, A. C., Nguyen, Q. C., McEwan, J. A., & Berget, I. (2021). Individual differences underlying food intake and liking in semisolid foods. *Food Quality and Preference, 87*, Article 104023.

Wang, M., Yao, M. N., Jian, W. J., Sun, Y. J., & Pang, J. (2010). Molecular dynamics simulations of the interactions between konjac glucomannan and soy protein isolate. *Agricultural Sciences in China, 9*(10), 1538–1542.

Wang, Y., Chen, Y., Zhou, Y., Nirasawa, S., Tatsumi, E., Li, X., & Cheng, Y. (2017). Effects of konjac glucomannan on heat-induced changes of wheat gluten structure. *Food Chemistry, 229*, 409–416.

Willett, W., Rockström, J., Loken, B., Springmann, M., Lang, T., Vermeulen, S., … Wood, A. (2019). Food in the Anthropocene: The EAT–Lancet Commission on healthy diets from sustainable food systems. *The Lancet, 393*(10170), 447–492.

Xiong, G., Cheng, W., Ye, L., Du, X., Zhou, M., Lin, R., Geng, S., Chen, M., Corke, H., & Cai, Y.-Z. (2009). Effects of konjac glucomannan on physicochemical properties of myofibrillar protein and surimi gels from grass carp (*Ctenopharyngodon idella*). *Food Chemistry, 116*(2), 413–418.

Xiong, Y., Li, Q., Miao, S., Zhang, Y., Zheng, B., & Zhang, L. (2019). Effect of ultrasound on physicochemical properties of emulsion stabilized by fish myofibrillar protein and xanthan gum. *Innovative Food Science & Emerging Technologies, 54*, 225–234.

Xu, W., Xiong, Y., Li, Z., Luo, D., Wang, Z., Sun, Y., & Shah, B. R. (2020). Stability, microstructural and rheological properties of complex prebiotic emulsion stabilized by sodium caseinate with inulin and konjac glucomannan. *Food Hydrocolloids, 105*, Article 105772.

Yang, D., Gao, S., & Yang, H. (2020). Effects of sucrose addition on the rheology and structure of iota-carrageenan. *Food Hydrocolloids, 99*, Article 105317.

Yang, D., Yuan, Y., Wang, L., Wang, X., Mu, R., Pang, J., … Zheng, Y. (2017). A review on konjac glucomannan gels: Microstructure and application. *International Journal of Molecular Sciences, 18*(11), 2250.

Yang, Z., Yang, H., & Yang, H. (2018). Effects of sucrose addition on the rheology and microstructure of κ-carrageenan gel. *Food Hydrocolloids, 75*, 164–173.

Yuliarti, O., Kovis, T. J. K., & Yi, N. J. (2021). Structuring the meat analogue by using plant-based derived composites. *Journal of Food Engineering, 288*, Article 110138.

Zhang, T., Xue, Y., Li, Z., Wang, Y., & Xue, C. (2015). Effects of deacetylation of konjac glucomannan on Alaska Pollock surimi gels subjected to high-temperature (120 °C) treatment. *Food Hydrocolloids, 43*, 125–131.

Zhou, Y., & Yang, H. (2019). Effects of calcium ion on gel properties and gelation of tilapia (*Oreochromis niloticus*) protein isolates processed with pH shift method. *Food Chemistry, 277*, 327–335.

Zhuang, X., Wang, L., Jiang, X., Chen, Y., & Zhou, G. (2021). Insight into the mechanism of myofibrillar protein gel influenced by konjac glucomannan: Moisture stability and phase separation behavior. *Food Chemistry, 339*, Article 127941.